Structural and Magnetochemical Properties of Mono-, Di-, and Trinuclear Manganese(III) Dithiolate Complexes

Jeffrey L. Seela,[1a] Michael J. Knapp,[1b] Kevin S. Kolack,[1a] Hsiu-Rong Chang,[1b] John C. Huffman,[1a] David N. Hendrickson,*,[1b] and George Christou*,[1a]

Department of Chemistry and Molecular Structure Center, Indiana University, Bloomington, Indiana 47405-4001, and Department of Chemistry-0358, University of California at San Diego, La Jolla, California 92093-0358

Aerial oxidation of Mn^{II}/ptt^{3-} (ptt^{3-} = propane-1,2,3-trithiolate) mixtures gives $[Mn_2(pttd)_2]^{2-}$, where $pttd^{4-}$ is the mono(disulfide) of ptt^{3-}. $(NEt_3Bz)_2[Mn_2(pttd)_2]$ (**2**) crystallizes in space group $P2_1/c$ with (at −158 °C) $a = 11.540(2)$ Å, $b = 12.115(2)$ Å, $c = 17.478(4)$ Å, $\beta = 101.78(1)°$, and $Z = 2$. The anion contains a doubly-bridged $[Mn_2S_8]$ core (Mn···Mn = 3.598(2) Å) with five-coordinate Mn^{III} ions, very similar to previously reported $[Mn_2(edt)_4]^{2-}$ (anion of **1**; edt^{2-} = ethane-1,2-dithiolate). Aerial oxidation of Mn^{II}/pdt^{2-} (pdt^{2-} = propane-1,3-dithiolate) mixtures gives $[Mn_3(pdt)_5]^{2-}$, which is mixed valent (Mn^{II}, $2Mn^{III}$). $(PPh_4)_2[Mn_3(pdt)_5]$ (**3**) crystallizes in space group $P\bar{1}$ with (at −161 °C) $a = 14.385(6)$ Å, $b = 23.734(11)$ Å, and $Z = 2$. The anion contains a near-linear $Mn^{III}Mn^{II}Mn^{III}$ unit with five-coordinate Mn^{III}, six-coordinate Mn^{II}, and three thiolate bridges between each Mn_2 pair; Mn···Mn separations are 3.123(3) and 3.101(3) Å. Aerial oxidation of $Mn^{II}/edt^{2-}/ImH$ (ImH = imidazole) mixtures gives $[Mn(edt)_2(ImH)]^-$. $(NEt_4)[Mn(edt)_2(ImH)]$ (**4**) crystallizes in space group $P2_1/n$ with (at −72 °C) $a = 13.974(5)$ Å, $b = 14.317(5)$ Å, $c = 10.564(3)$ Å, $\beta = 90.13(2)°$, and $Z = 4$. The anion is five-coordinate and square-pyramidal. Aerial oxidation of $Mn^{II}/edt^{2-}/Im^-$ mixtures gave $[Mn_2(Im)(edt)_4]^{3-}$, which contains two Mn^{III} ions. $(NMe_4)_3[Mn_2(Im)(edt)_4]$ (**5**) crystallizes in space group $Pna2_1$ with (at −160 °C) $a = 17.965(5)$ Å, $b = 16.094(4)$ Å, $c = 14.789(3)$ Å, and $Z = 4$. The five-coordinate Mn^{III} ions are bridged by the Im^- group across a Mn···Mn separation of 6.487(2) Å. The anion of **4** contains high-spin Mn^{III} ($S = 2$) and exhibits inter-anion antiferromagnetic exchange interactions ($J = -0.15$ cm^{-1}, $g = 1.91$) propagated by interanion NH···S hydrogen bonds. Complexes **1**−**3** and **5** all possess intraanion antiferromagnetic exchange interactions; the fitting parameters are as follows: **1**, $J = -19.0$ cm^{-1}, $g = 1.96$, $D = -0.22$ cm^{-1}; **2**, $J = -16.4$ cm^{-1}, $g = 1.96$, $D = -0.22$ cm^{-1}; **3**, $J = -18.8$ cm^{-1}, $g = 2.00$; **5**, $J = -1.75$ cm^{-1}, $g = 1.84$, $D = -0.028$ cm^{-1} ($\hat{H} = -2JS_iS_j$ convention). Complexes **1**, **2**, and **5** have $S = 0$ ground states, while that of **3** is $S = \frac{3}{2}$.

Introduction

Manganese(III) chemistry is proving to be a rich source of polynuclear complexes with a variety of interesting structural and physical properties. One such property is an unusually large value of spin (S) in the ground state,[2−7] a result of the presence of (at least some) ferromagnetic exchange interactions between the constituent paramagnetic metal ions and/or the presence of spin frustration[8,9] effects arising in certain topological arrangements of metal ions possessing competing pairwise exchange interactions of comparable magnitude. More recently, a subset

of high-spin molecules has emerged that has been termed "single-molecule magnets"; such compounds display superparamagnet-like frequency-dependent out-of-phase signals in AC susceptibility studies that are the signature of slow relaxation of the magnetization. At low enough temperatures, these molecules can consequently function as magnetizable magnets.[3−7,10−12] These molecules currently include the mixed-valent $[Mn_{12}O_{12}(O_2CR)_{16}(H_2O)_4]^{0,-}$ and $[Mn_4O_3X(O_2CR)_3$-

(1) (a) Indiana University. (b) University of California.

(2) Tsai, H.-L.; Wang, S.; Folting, K.; Streib, W. E.; Hendrickson, D. N.; Christou, G. *J. Am. Chem. Soc.* **1995,** *117*, 2503.

(3) Sessoli, R.; Tsai, H.-L.; Schake, A. R.; Wang, S.; Vincent, J. B.; Folting, K.; Gatteschi, D.; Christou, G.; Hendrickson, D. N. *J. Am. Chem. Soc.* **1993,** *115*, 1804.

(4) Christou, G. In *Magnetism: A Supramolecular Function*; Kahn, O., Ed.; NATO ASI Series; Kluwer Academic Publishers: Dordrecht, The Netherlands, 1996; pp 383−410.

(5) Tsai, H.-L.; Hendrickson, D. N.; Eppley, H. J.; de Vries, N.; Folting, K.; Christou, G. *J. Chem. Soc., Chem. Commun.* **1994,** 1745.

(6) Eppley, H. J.; Wang, S.; Tsai, H.-L.; Aubin, S. A.; Folting, K.; Streib, W. E.; Hendrickson, D. N.; Christou, G. *Mol. Cryst. Liq. Cryst.* **1995,** *274*, 159.

(7) Bolcar, M. A.; Aubin, S. M. J.; Folting, K.; Hendrickson, D. N.; Christou, G. *Chem. Commun.* **1997,** 1485.

(8) In accord with the suggestion by Kahn,[9] we shall employ the term "degenerate spin frustration" for the important situation where competing exchange interactions result in an orbitally degenerate ground state. We shall therefore continue to employ the term "spin frustration" for the more general situation where competing exchange interactions of comparable magnitude lead to the prevention (frustration) of preferred spin alignments.

(9) Kahn, O. *Chem. Phys. Lett.* **1997,** *265*, 109.

(10) Sessoli, R.; Gatteschi, D.; Caneschi, A.; Novak, M. A. *Nature* **1993,** *365*, 141.

(11) (a) Eppley, H. J.; Aubin, S. M. J.; Wemple, M. W.; Adams, D. M.; Tsai, H.-L.; Castro, S. L.; Sun, Z.; Folting, K.; Huffman, J. C.; Hendrickson, D. N.; Christou, G. *Mol. Cryst. Liq. Cryst.* **1997,** *305*, 167. (b) Aubin, S. M. J.; Spagna, S.; Eppley, H. J.; Folting, K.; Christou, G.; Hendrickson, D. N. *Mol. Cryst. Liq. Cryst.* **1997,** *305*, 181.

(12) (a) Hendrickson, D. N.; Adams, D. M.; Wu, C.-C.; Aubin, S. M. J. In *Magnetism: A Supramolecular Function*; Kahn, O, Ed.; NATO ASI Series; Kluwer Academic Publishers: Dordrecht, The Netherlands, 1996; pp 357−382. (b) Gatteschi, D.; Sessoli, R. *Ibid.*, pp 411−430.

(dbm)$_3$] (various X and R groups) families of complexes, among others.[3–7,10–12] It is recognized that these unusual properties require a combination of large enough S and zero-field splitting parameter D, the latter needing also to be negative: this is a result of the barrier to relaxation being $|S^2D|$ or $|(S^2 - {}^1/_4)D|$ for integer and half-integer spins, respectively.

With the new phenomenon identified, a search for new examples of such molecules is in progress, both in Mn^{III} chemistry and elsewhere. Several years ago, we and others briefly reported the synthesis of the first examples of stable Mn^{III} thiolate complexes.[13–15] More recently, we have returned to magnetochemically characterize these molecules in detail with a particular emphasis on the ground state S and D values to be encountered in this area. We herein describe the syntheses, full structural details, and magnetochemical properties of several of these species spanning nuclearities 1 to 3 and at the oxidation level Mn^{III} or mixed-valent Mn^{II}, Mn^{III}.

Experimental Section

Syntheses. All manipulations were carried out under a dinitrogen atmosphere using standard Schlenk and glovebox techniques. Solvents were distilled from CaH$_2$ (MeCN) or Na/benzophenone (Et$_2$O, THF); anhydrous EtOH and *N,N*-dimethylformamide (DMF) were routinely stored over molecular sieves. Ethane-1,2-dithiol (edtH$_2$), propane-1,3-dithiol (pdtH$_2$), propane-1,2,3-trithiol (pttH$_3$), and imidazole (ImH) were used as received.

(NEt$_4$)$_2$[Mn$_2$(edt)$_4$] (1). Ethane-1,2-dithiol (3.35 mL, 40 mmol) was introduced via syringe into a solution of sodium metal (1.84 g, 80.0 mmol) in EtOH (200 mL). To this were added NEt$_4$Br (8.40 g, 40.0 mmol) and MnCl$_2$·4H$_2$O (3.96 g, 20.0 mmol) dissolved in EtOH (30 mL) to yield a slurry of a fine white solid. The mixture was stirred vigorously while small portions of air were successively added using a syringe needle through the septum cap and partial evacuation of the reaction flask. A deep green color was rapidly generated, followed by appearance of a black microcrystalline solid. Addition of air was continued until the majority of the white solid had dissolved and no more green color was generated. At this point, anaerobic conditions were reestablished and the black solid was collected by filtration, washed with additional EtOH, and dried *in vacuo*. The crude solid was dissolved in warm CH$_3$CN (~60 °C, 340 mL), the solution was filtered, and THF (120 mL) was added. The solution was maintained at −20 °C overnight, and the resulting black prisms were collected by filtration, washed with THF, and dried *in vacuo*. Yields as high as 50% (3.7 g) have been routinely obtained. Anal. Calcd (found) for C$_{24}$H$_{56}$N$_2$S$_8$Mn$_2$: C, 39.00 (39.21); H, 7.64 (7.73); N, 3.79 (3.81); S, 34.71 (34.75). Electronic spectrum in DMF (1.40 mM) [λ_{max}, nm (ϵ_M, L mol^{-1} cm^{-1})]: 589 (500), 395 (6900), 352 (15 000), 295 (3800).

(NEt$_3$Bz)$_2$[Mn$_2$(pttd)$_2$] (2). Propane-1,2,3-trithiol (4.40 mL, 40 mmol) was introduced via syringe into a solution of sodium metal (2.76 g, 120 mmol) in EtOH (150 mL). To this were added NEt$_3$BzBr (6.82 g, 30.0 mmol) and anhydrous MnCl$_2$ (2.52 g, 20.0 mmol) to yield a slurry of white solid. Aerial oxidation was carried out as described for **1**. A deep green color was rapidly generated, and continued additions of air resulted in the appearance of a fine green powder. Addition of air was discontinued when the solution became light green in color, whereupon anaerobic conditions were reestablished. The green precipitate was collected via filtration, washed well with EtOH, and dried *in vacuo*. The crude solid was dissolved in warm CH$_3$CN (50

°C, 150 mL), the solution was filtered, and an equal volume of Et$_2$O was added. The solution was maintained at −20 °C overnight, and the resulting black crystals were collected by filtration, washed with Et$_2$O, and dried *in vacuo*. Yields were routinely ~35% (3.6 g). Similar recrystallization of the crude product from DMF/Et$_2$O gave black crystals in 40% yield suitable for an X-ray diffraction study. Anal. Calcd (found) for C$_{38}$H$_{64}$N$_2$S$_{12}$Mn$_2$: C, 43.74 (43.59); H, 6.18 (6.26); N, 2.68 (2.79); S, 36.87 (36.76). Electronic spectrum in DMF (1.47 mM): 654 (710), 410 (sh, 7250), 340 (9000), 310 (sh, 5500).

(PPh$_4$)$_2$[Mn$_3$(pdt)$_5$] (3). A reaction solution was prepared as described for **1** containing sodium metal (1.38 g, 60.0 mmol), 1,3-propanedithiol (3.01 mL, 30.0 mmol), anhydrous MnCl$_2$ (1.89 g, 15.0 mmol), and PPh$_4$Br (6.3 g, 15 mmol) in EtOH (135 mL). The resulting white slurry was stirred vigorously while controlled aerial oxidation was carried out as described for **1**. Rapid formation of a deep green color was observed, followed closely by precipitation of a black microcrystalline solid. Anaerobic conditions were reestablished when no more green color was generated, and the precipitated product was collected by filtration, washed with cold EtOH (20 mL), and dried *in vacuo*. The solid was dissolved in DMF at ambient temperature (150 mL), the solution was filtered, and the filtrate was concentrated to *ca.* 75 mL by removal of solvent under vacuum. Addition of Et$_2$O (50 mL), and storage overnight at −20 °C gave the product as well-formed black crystals, which were collected by filtration, washed with CH$_3$-CN (2 × 10 mL) and Et$_2$O (20 mL), and dried *in vacuo* (yield 36%). Anal. Calcd (found) for **3**·2H$_2$O (C$_{63}$H$_{74}$O$_2$S$_{10}$P$_2$Mn$_3$): S, 22.73 (22.66); C, 53.64 (53.39); H, 5.29 (5.56). Electronic spectrum in DMF (1.54 mM): 410 (sh, 4420), 368 (5650).

(NEt$_4$)[Mn(edt)$_2$(ImH)] (4). Ethane-1,2-dithiol (3.35 mL, 40 mmol) was introduced *via* syringe into a solution of sodium metal (1.84 g, 80.0 mmol) in EtOH (250 mL). To this were added NEt$_4$Br (12.6 g, 60.0 mmol), imidazole (5.45 g, 80.0 mmol), and MnCl$_2$·4H$_2$O (3.96 g, 20.0 mmol) to yield a slurry of a fine white solid. The mixture was stirred vigorously while small portions of air were successively added using a syringe needle through the septum cap and partial evacuation of the reaction flask. A deep green color was rapidly generated, followed by appearance of a black microcrystalline solid. Addition of air was continued until the majority of the white solid had dissolved and no more green color was generated. At this point, anaerobic conditions were reestablished and the black microcrystals collected by filtration, washed well with EtOH, and dried *in vacuo*. The crude solid was dissolved in warm MeCN (~35 °C, ~300 mL), the solution was filtered, and an equal volume of THF was added. The solution was maintained at −20 °C overnight, and the resulting black prisms were collected by filtration, washed well with THF, and dried *in vacuo*. Yields as high as 90% (7.9 g) have been routinely obtained by this method. Anal. Calcd (found) for C$_{15}$H$_{32}$N$_3$S$_4$Mn: C, 41.17 (41.50); H, 7.37 (7.20); N, 9.60 (9.81). Electronic spectrum in MeCN (2.67 mM) [λ_{max} (ϵ_M)]: 290 sh (4490), 355 (13 300), 390 sh (6740), 610 (545).

(NMe$_4$)$_3$[Mn$_2$(Im)(edt)$_4$] (5). Ethane-1,2-dithiol (1.68 mL, 20.0 mmol) and imidazole (2.72 g, 40.0 mmol) were dissolved in a solution of sodium metal (1.84 g, 80.0 mmol) in EtOH (125 mL). To this were added NMe$_4$Cl (3.29 g, 30.0 mmol) and anhydrous MnCl$_2$ (1.26 g, 10.0 mmol), and the mixture was cooled to 0 °C in an ice bath. Aerial oxidation was performed as for **1**, and a deep green color was rapidly generated, followed by precipitation of a green powder. Anaerobic conditions were reestablished, and the green powder was collected by filtration, washed with cold EtOH (2 × 10 mL), and dried *in vacuo*. The solid was dissolved in warm DMF (~45 °C), the solution was filtered, and ~1.5 volumes of THF were added. The solution was maintained overnight at −20 °C to yield black prisms, which were collected by filtration, washed with THF and dried *in vacuo*. Yields of 40–50% have been obtained. Anal. Calcd (found) for C$_{23}$H$_{55}$N$_5$S$_8$-Mn$_2$: 35.97 (35.99); H, 7.22 (7.43); N, 9.12 (8.92). This material was found unsuitable for crystallograpahy. However, **5** can be recrystallized from warm MeCN to yield well-formed crystals of **5**·2MeCN, and these were found suitable for structural studies. Electronic spectrum in DMF (3.45 mM): 312 (3340), 375 (9200), 426 (4980), 646 (375).

X-ray Crystallography. Data were collected on complexes **2**–**5**·2MeCN using a Picker four-circle diffractometer; details of the

(13) (a) Christou, G.; Huffman, J. C. *J. Chem. Soc., Chem. Commun.* **1983**, 558. (b) Christou, G.; Hagen, K. S.; Bashkin, J. K.; Holm, R. H. *Inorg. Chem.* **1985**, *24*, 1010. (c) Seela, J. L.; Folting, K.; Wang, R.-J.; Huffman, J. C.; Christou, G.; Chang, H.-R.; Hendrickson, D. N. *Inorg. Chem.* **1985**, *24*, 4454.

(14) (a) Costa, T.; Dorfman, J. R.; Hagen, K. S.; Holm, R. H. *Inorg. Chem.* **1983**, *22*, 4091. (b) Pulla Rao, Ch; Dorfman, J. R.; Holm, R. H. *Inorg. Chem.* **1986**, *25*, 428.

(15) (a) Henkel, G.; Greiwe, K.; Krebs, B. *Angew. Chem., Int. Ed. Engl.* **1985**, *24*, 117. (b) Greiwe, K.; Krebs, B.; Henkel, G. *Inorg. Chem.* **1989**, *28*, 3713.

Table 1. Crystallographic Data for Complexes **2**−**5**

	2	**3**	**4**	**5**[a]
formula	$C_{38}H_{64}N_2S_{12}Mn_2$	$C_{63}H_{70}P_2S_{10}Mn_3$	$C_{15}H_{32}N_3S_4Mn$	$C_{27}H_{61}N_7S_8Mn_2$[a]
fw	1043.53	1374.61	437.62	850.18
space group	$P2_1/c$	$P\bar{1}$	$P2_1/n$	$Pna2_1$
a, Å	11.540(2)	14.385(6)	13.974(5)	17.965(5)
b, Å	12.115(2)	23.734(11)	14.317(5)	16.094(4)
c, Å	17.478(4)	9.881(3)	10.564(3)	14.789(3)
α, deg	90	100.39(2)	90	90
β, deg	101.78(1)	93.25(2)	90.13(2)	90
γ, deg	90	107.53(2)	90	90
V, Å^3	2392	3142	2114	4276
Z	2	2	4	4
T, °C	−158	−161	−72	−160
radiation, Å[b]	0.710 69	0.710 69	0.710 69	0.710 69
ρ_{calc}, g/cm^3	1.449	1.453	1.375	1.321
μ, cm^{-1}	10.404	9.784	9.824	9.698
R (R_w), %	3.59 (3.94)	6.41 (6.06)	5.86 (5.80)	4.58 (4.40)

[a] Including 2 MeCN molecules. [b] Graphite monochromator. [c] $R = 100 \sum ||F_o| - |F_c||/\sum |F_o|$. [d] $R_w = 100 [\sum w(|F_o| - |F_c|)^2/\sum w|F_o|^2]^{1/2}$, where $w = 1/\sigma^2(|F_o|)$.

diffractometry, low-temperature facilities, and computational procedures employed by the Molecular Structure Center are available elsewhere.[16] Suitable crystals were located using inert-atmosphere handling techniques, and they were affixed to glass fibers using silicone grease and transferred to a goniostat where they were cooled for characterization and data collection. The structures wee solved by direct methods (MULTAN) and standard Fourier techniques and refined on F by full-matrix least-squares cycles. No absorption corrections were performed.

For complex **2** ($+h,+k,\pm l$; $6° \leq 2\theta \leq 45°$) a systematic search of a limited hemisphere of reciprocal space revealed a monoclinic lattice with systematic extinctions corresponding to the unique space group $P2_1/c$. Subsequent successful solution and refinement of the structure confirmed this choice. All non-hydrogen atoms were readily located, and no disorder problems were encountered. All hydrogen atoms were observed in a difference Fourier map phased on the non-hydrogen atoms and were refined with isotropic thermal parameters in the final refinement cycles; non-hydrogen atoms were refined with anisotropic thermal parameters. The final difference Fourier map was essentially featureless, the largest peak being less than 0.5 e/Å^3.

For complex **3** ($+h,\pm k,\pm l$; $6° \leq 2\theta \leq 45°$), a systematic search of a limited hemisphere of reciprocal space located a set of diffraction maxima with no symmetry of systematic absences, thus indicating a triclinic space group. Subsequent successful solution and refinement of the structure confirmed the choice of $P\bar{1}$. All non-hydrogen atoms were readily located with no major disorder problems being encountered. Owing to the number of independent atoms, all atoms in the anion were refined anisotropically, as well as the phosphorus atoms. Carbon atoms of the PPh$_4^+$ cations were refined isotropically, while all hydrogen atoms were placed in fixed, idealized positions. The thermal parameters associated with C(26) and C(27) are highly anisotropic (see Supporting Information) and suggest that in fact there may be some slight disorder present. No attempt was made to resolve such a disorder, and the final difference Fourier map was essentially featureless.

For complex **4** ($+h,+k,\pm l$; $6° \leq 2\theta \leq 45°$), a systematic search of a limited hemisphere of reciprocal space revealed a monoclinic lattice with extinctions corresponding to the unique space group $P2_1/n$. Data were collected in the usual manner, although it was noticed that several of the located peaks were somewhat broad. After data collection, the structure was successfully solved; however, although difference Fourier maps were generally featureless, the residuals failed to drop below 0.14, even after anisotropic refinement. The crystal was then carefully examined and discovered to undergo an apparent phase transition near −160 °C. For this reason, a second sample was mounted and characterized at −72 °C. The cell parameters differ only slightly (at

−160 °C: $a = 13.927(4)$ Å, $b = 14.246(4)$ Å, $c = 10.540(3)$ Å, $\beta = 90.28(2)°$), but at the higher temperature, the peaks were all well-formed and quite sharp. Refinement using data collected at −72 °C converged rapidly. All hydrogen atoms were located in a difference Fourier map and included in the final cycles of refinement. A final difference Fourier map was essentially featureless, the largest peak being 0.23 e/Å^3.

For complex **5**·2MeCN ($+h,+k,+l$; $6° \leq 2\theta \leq 45°$), a systematic search of a limited hemisphere of reciprocal space located a set of diffraction maxima with orthorhombic symmetry and extinctions consistent with space group $Pna2_1$ or $Pnam$. Statistical tests strongly indicated the noncentric space group $Pna2_1$, and successful solution and refinement of the structure confirmed this choice. All non-hydrogen atoms were readily located and refined with anisotropic thermal parameters. Hydrogen atoms were, in general, clearly visible in a difference Fourier map phased on the non-hydrogen atoms, with the exception of those associated with the two solvent molecules. The hydrogen atoms associated with the anion were allowed to vary isotropically in the final cycles, while all others were included only as fixed, idealized contributors. A final difference Fourier map was essentially featureless, the largest peak being 0.45 e/Å^3.

For all complexes, the data collection and structure solution parameters are listed in Table 1, together with standard discrepancy indices R and R_w.

Physical Measurements. Variable-temperature magnetic susceptibility data were measured using a series 800 VTS-50 SQUID susceptometer (SHS Corp.). The susceptometer was operated at a magnetic field strength of 10 kG. Samples were loaded in an inert-atmosphere box and transferred quickly to the SQUID susceptometer where the samples were maintained under a helium atmosphere. Diamagnetic corrections were estimated from Pascal's constants and subtracted from the experimental susceptibility data to obtain the molar paramagnetic susceptibilities of the complexes, which were then fit to the appropriate theoretical expressions derived as described in the text. Solution magnetic susceptibilities were obtained using the Evans method[17] in (CD$_3$)$_2$SO containing SiMe$_4$ (1−2% v/v). Electronic spectra were recorded on a Hewlett Packard 8452A spectrophotometer.

Results

Syntheses. The formation of stable Mn^{III}/thiolate complexes was first demonstrated with edt^{2-} giving the [Mn$_2$(edt)$_4$]$^{2-}$ ion.[13a,14a] Extension of this approach to other dithiolates led to cocrystallized [Mn(tdt)$_2$]$^-$/[Mn(tdt)$_2$(MeOH)]$^-$ (tdt^{2-} = toluene-3,4-dithiolate)[15] and the complexes described herein.[14b,c] Our own efforts were additionally directed toward assessing the influence of the chelate ring size on the stability of the resultant

(16) Chisholm, M. H.; Folting, K.; Huffman, J. C.; Kirkpatrick, C. C. *Inorg. Chem.* **1984**, *23*, 1021.

(17) Evans, D. F. *J. Chem. Soc.* **1959**, 2003.

product to the redox reaction of eq 1 and to see if the use of trithiolate might lead to products with a nuclearity greater than two.

$$Mn^{III} + RS^- \rightarrow Mn^{II} + {}^1\!/_2 RSSR \qquad (1)$$
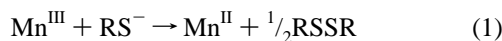
Use of propane-1,2,3-trithiolate (ptt^{3-}) also led to a stable deep green product on aerial oxidation of the parent Mn^{II} reaction mixture, but the product anion [Mn$_2$(pttd)$_2$]$^{2-}$ of **2** was essentially the same as **1** with the third S being oxidized to a disulfide bridge to give the tetrathiolate, disulfide ligand pttd^{4-}. A different result was obtained with propane-1,3-dithiolate (pdt^{2-}) whose six-membered chelate ring also gave a stable deep green color, but the product [Mn$_3$(pdt)$_5$]$^{2-}$ anion of **3** was now trinuclear and mixed-valent (Mn^{II}, 2Mn^{III}). It has less thermal stability than **1** or **2** in solution, and all manipulations must be performed at room temperature to avoid the bleaching of the color characteristic of reduction to Mn^{II} (eq 1). Use of NEt$_4^+$ in place of PPh$_4^+$ does not lead to precipitation of the deep green anion from solution and leads to bleaching of the deep green color within a few minutes, even at ice-bath temperatures.

Aerial oxidation of reaction solutions containing butane-1,4-dithiolate also leads to deep green colors, but the color fades within seconds, supporting a decrease in stability with increasing chain length. Thus, the edt^{2-} group leads to the most stable Mn^{III}/RS$^-$ product. The use of the related ligand propane-1,2-dithiolate (pdt′) gives a [Mn$_2$(pdt′)$_4$]$^{2-}$ product essentially identical to **1** and **2**.[18] Use of the bulky monothiolate C$_6$H$_2$(Pr^i)$_3$S$^-$ with Pr^i substituents in the 2, 4, and 6 positions gives a Mn^{III} product which is thought to be a square-planar mononuclear system, analogous to [Mn(tdt)$_2$]$^-$, but the thermal instability of the former has hindered further characterization.[19]

Other chelates containing thiolate groups and capable of forming five-membered chelate rings have also been explored: These include XCH$_2$CH$_2$SH (X = NH$_2$, OH) and HSCH$_2$CO$_2$H. In all cases, intense colors were generated at the aerial oxidation step, but these faded within minutes at ice-bath temperatures. This is in contrast to the use of thiosalicylate (thiosal^{2-}), i.e. 2-mercaptobenzoate, which forms six-membered chelate rings and yields a stable, mononuclear Mn^{III} product, [Mn(thiosal)$_2$-(ImH)]$^-$.[20]

The observation[13,14] that the anion of **1** dissociates into solvated monomers when dissolved in good donor solvents such as DMF and DMSO (eq 2) led us to suspect that the better donor

$$[Mn_2(edt)_4]^{2-} + 2n \text{ solv} \rightleftharpoons 2[Mn(edt)_2(solv)_n]^- \quad (n = 1, 2)$$
$$(2)$$
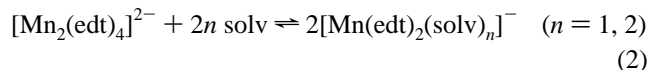
ImH might be capable of trapping the monomer as its ImH adduct and allowing its isolation. Indeed, **4** was originally made[13b] by treatment of **1** with 10 equiv of ImH in DMF, followed by precipitation with acetone and recrystallization from MeCN/THF (eq 3). Recrystallization of **4** from DMF/THF

$$\mathbf{1} \xrightarrow{\text{DMF}} [Mn(edt)_2(DMF)_n]^- \xrightarrow[\text{excess}]{\text{ImH}} \mathbf{4} \quad (n = 1, 2) \quad (3)$$
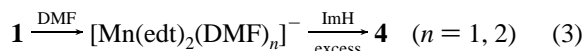
yielded crystals of **1**, showing that the binding of ImH is reversible in good donor solvents. We subsequently developed a high yield, one-pot synthesis of **4**, as described in the

(18) Chen, X.; Kang, B.; Weng, L.; Huang, L.; Liu, H.; Wu, D.; Lei, X.; Hong, M.; Lu, J. *Transition Met. Chem.* **1992**, *17*, 509.
(19) Fikar, R.; Koch, S. A.; Millar, M. M. *Inorg. Chem.* **1985**, *24*, 3311.
(20) Bashkin, J. S.; Huffman, J. C.; Christou, G. *J. Am. Chem. Soc.* **1986**, *108*, 5038.
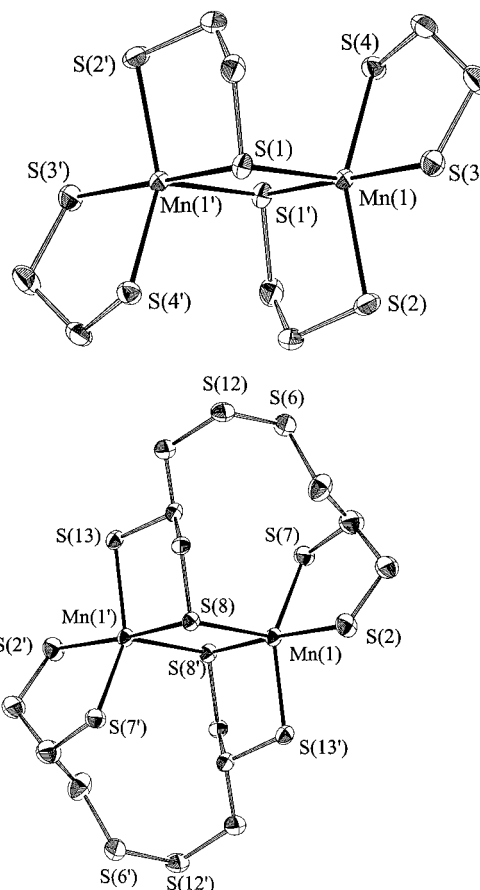
Figure 1. ORTEP representations of the anions of **1** (top) and **2** (bottom) at the 50% probability level. Primed and unprimed atoms are related by an inversion center.

Experimental Section, that does not require prior isolation of **1**. Thus, aerial oxidation of Mn^{II}/edt^{2-} reaction mixtures in the presence of imidazole leads directly to precipitation of **4** if NEt$_4^+$ is present.

The anion of complex **5** was originally prepared from that of **4** by treatment with 0.5 equiv of NaOEt to deprotonate half the imidazole −NH groups and induce dimerization (eq 4).

$$2[Mn(edt)_2(ImH)]^- + NaOEt \xrightarrow[\text{EtOH}]{\text{MeCN}}$$
$$[Mn_2(Im)(edt)_4]^{3-} + Na^+ + EtOH + ImH \quad (4)$$
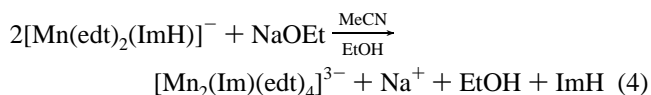
However, we soon developed a high-yield one-pot synthesis to this complex also, as described in the Experimental Section. Thus, NaIm is prepared *in situ* in the reaction flask prior to aerial oxidation, and this leads to clean precipitation of **5** after addition of air. In contrast to **4**, complex **5** can be recrystallized from DMF/THF, attesting to the stronger binding of imidazolate *vs* imidazole to the positively charged metal centers. This is consistent with the shorter Mn−N distances in **5** *vs* **4** (*vide infra*).

Complexes **1**−**5** are oxygen-sensitive in solution but much less so in the solid state, and brief (a few minutes) exposure of solid material to air has been found not to be detrimental.

Description of Structures. ORTEP diagrams of **1**−**5** are presented in Figures 1−5, and selected interatomic distances and angles for **2**−**5** are listed in Tables 2−5; the structure of **1** has already been described in detail elsewhere.[13,14]

The [Mn$_2$(pttd)$_2$]$^{2-}$ ion of imposed C_i symmetry is very similar to the [Mn$_2$(edt)$_4$]$^{2-}$ ion (Figure 1). Two adjacent S

Figure 2. ORTEP representation of the anion of **3** at the 50% probability level. The C atoms between S(24) and S(28) have large thermal ellipsoids suggesting some disorder and are represented for convenience as isotropic spheres of arbitrary size.

Figure 3. ORTEP representation of the anion of **4** at the 50% probability level.

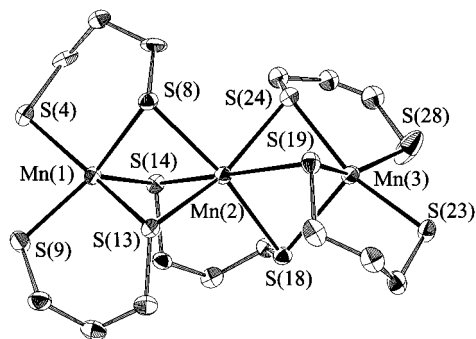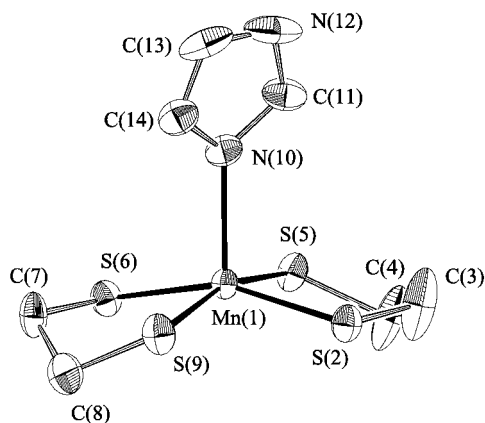**Figure 4.** Interanion NH···S hydrogen-bonding arrangement in **4** leading to 1-D chains in the solid state.

Figure 5. ORTEP representation of the anion of **5** at the 50% probability level.

Table 2. Selected Bond Distances (Å) and Angles (deg) for (NEt₃Bz)₂[Mn₂(pttd)₂] (**2**)

Mn(1)−Mn(1′)	3.598(2)	S(6)−S(12)	2.041(2)
Mn(1)−S(2)	2.322(1)	Mn(1)−S(8′)	2.353(1)
Mn(1)−S(7)	2.329(1)	Mn(1)−S(13)	2.317(1)
Mn(1)−S(8)	2.655(1)		
S(2)−Mn(1)−S(7)	88.74(4)	S(7)−Mn(1)−S(8′)	89.95(4)
S(2)−Mn(1)−S(8)	98.00(4)	S(7)−Mn(1)−S(13′)	144.53(5)
S(2)−Mn(1)−S(8′)	173.45(5)	S(8)−Mn(1)−S(8′)	88.35(4)
S(2)−Mn(1)−S(13′)	88.55(4)	S(8)−Mn(1)−S(13′)	99.61(4)
S(7)−Mn(1)−S(8)	115.79(5)	S(8′)−Mn(1)−S(13′)	88.79(4)
Mn(1)−S(8)−Mn(1′)	91.65(4)		

atoms of the initially ptt³⁻ group have acted like those in an edt²⁻ group and assembled a [Mn₂S₈] core identical to that in **1**. The remaining four thiolate groups have been oxidized to give two interligand disulfide bonds converting the ptt³⁻ groups to pttd⁴⁻; the ligands in the anion of **2** are thus best described as two binucleating tetrathiolates. Comparison of metric parameters shows near congruency in **1** and **2** of those portions common to both anions. The main differences are in the Mn···Mn separations (3.598(2) *vs* 3.543(2) Å in **2** *vs* **1**) and the resultant Mn−S$_{br}$ distances (2.353(1), 2.655(1) Å for **2**; 2.341(2), 2.606(2) Å for **1**). The extent to which these differences affect the exchange interactions between the Mn^{III} ions is considered below. The Mn^{III} geometries are essentially intermediate between square-pyramidal (sp) and trigonal bipyramidal (tbp) with a τ value of 0.48 ($\tau = 0$ and 1 for sp and tbp geometries, respectively).[21]

In the anion of complex **3** (Figure 2), the three Mn ions are nearly linear (169.7(1)°). The anion possesses C_2 virtual symmetry, with the C_2 axis passing through Mn(2) and C(16) (the central C atom of the pdt²⁻ ligand containing S(14) and S(18)). Charge considerations require a mixed-valence Mn^{II}, 2Mn^{III} description, and central Mn(2) is readily assigned as the Mn^{II} ion and Mn(1) and Mn(3) as the Mn^{III} ions on the basis of their structural parameters. Mn(2) is six-coordinate and approximately octahedral, while Mn(1) and Mn(3) are five-coordinate with a geometry that approximates to sp ($\tau = 0.15$ and 0.16 for Mn(1) and Mn(3), respectively) with S(14) and S(18) in the axial positions, rather than intermediate between

(21) Addison, A. W.; Rao, T. N.; Reedijk, J.; Rijn, J.; Verschoor, G. C. *J. Chem. Soc., Dalton Trans.* **1984**, 1349.

sp and tbp as in **2**. Terminal Mn^{III}−S distances (2.315(3)− 2.327(3) Å) are similar to those in **2**, supporting the Mn^{III} description for these ions. The Mn···Mn separations (~3.1 Å) are much shorter than those in **1** and **2** (~3.6 Å) owing to the

Table 3. Selected Bond Distances (Å) and Angles (deg) for (PPh$_4$)$_2$[Mn$_3$(pdt)$_5$] (**3**)

Mn(1)...Mn(2)	3.123(3)	Mn(2)...Mn(3)	3.101(3)
Mn(1)−S(4)	2.315(3)	Mn(2)−S(18)	2.554(3)
Mn(1)−S(8)	2.380(3)	Mn(2)−S(19)	2.677(3)
Mn(1)−S(9)	2.327(3)	Mn(2)−S(24)	2.585(3)
Mn(1)−S(13)	2.375(3)	Mn(3)−S(18)	2.523(3)
Mn(1)−S(14)	2.512(3)	Mn(3)−S(19)	2.394(3)
Mn(2)−S(8)	2.673(3)	Mn(3)−S(23)	2.323(3)
Mn(2)−S(13)	2.607(3)	Mn(3)−S(24)	2.363(3)
Mn(2)−S(14)	2.581(3)	Mn(3)−S(28)	2.325(3)

Mn(1)−Mn(2)−Mn(3)	169.7(1)	S(14)−Mn(2)−S(19)	166.73(8)
S(4)−Mn(1)−S(8)	95.17(9)	S(14)−Mn(2)−S(24)	99.78(8)
S(4)−Mn(1)−S(9)	83.25(9)	S(18)−Mn(2)−S(19)	82.51(8)
S(4)−Mn(1)−S(13)	162.26(9)	S(18)−Mn(2)−S(24)	92.49(8)
S(4)−Mn(1)−S(14)	100.63(9)	S(19)−Mn(2)−S(24)	69.79(8)
S(8)−Mn(1)−S(9)	153.33(9)	S(18)−Mn(3)−S(19)	89.10(9)
S(8)−Mn(1)−S(13)	78.74(8)	S(18)−Mn(3)−S(23)	97.41(9)
S(8)−Mn(1)−S(14)	92.06(9)	S(18)−Mn(3)−S(24)	98.84(9)
S(9)−Mn(1)−S(13)	94.72(9)	S(18)−Mn(3)−S(28)	117.25(12)
S(9)−Mn(1)−S(14)	114.45(9)	S(19)−Mn(3)−S(23)	96.16(9)
S(13)−Mn(1)−S(14)	96.25(8)	S(19)−Mn(3)−S(24)	78.53(9)
S(8)−Mn(2)−S(13)	69.66(8)	S(19)−Mn(3)−S(28)	153.30(12)
S(8)−Mn(2)−S(14)	84.16(8)	S(23)−Mn(3)−S(24)	162.81(10)
S(8)−Mn(2)−S(18)	171.48(8)	S(23)−Mn(3)−S(28)	85.20(10)
S(8)−Mn(2)−S(19)	104.39(8)	S(24)−Mn(3)−S(28)	92.33(10)
S(8)−Mn(2)−S(24)	94.60(8)	Mn(1)−S(8)−Mn(2)	76.36(7)
S(13)−Mn(2)−S(14)	89.11(8)	Mn(1)−S(13)−Mn(2)	77.73(7)
S(13)−Mn(2)−S(18)	104.14(8)	Mn(1)−S(14)−Mn(2)	75.88(7)
S(13)−Mn(2)−S(19)	103.30(8)	Mn(2)−S(18)−Mn(3)	75.30(7)
S(13)−Mn(2)−S(24)	161.19(9)	Mn(2)−S(19)−Mn(3)	75.17(8)
S(14)−Mn(2)−S(18)	89.99(8)	Mn(2)−S(24)−Mn(3)	77.48(8)

Table 4. Selected Bond Distances (Å) and Angles (deg) for (NEt$_4$)[Mn(edt)$_2$(ImH)] (**4**)

Mn(1)−S(2)	2.319(3)	Mn(1)−S(9)	2.329(3)
Mn(1)−S(5)	2.334(3)	Mn(1)−N(10)	2.224(7)
Mn(1)−S(6)	2.330(3)		

S(2)−Mn(1)−S(5)	89.13(13)	S(5)−Mn(1)−S(9)	164.28(9)
S(2)−Mn(1)−S(6)	157.60(9)	S(5)−Mn(1)−N(10)	97.02(18)
S(2)−Mn(1)−S(9)	88.17(13)	S(6)−Mn(1)−S(9)	88.16(12)
S(2)−Mn(1)−N(10)	102.88(18)	S(6)−Mn(1)−N(10)	99.52(19)
S(5)−Mn(1)−S(6)	88.46(12)	S(9)−Mn(1)−N(10)	98.68(19)

Table 5. Selected Bond Distances (Å) and Angles (deg) for (NMe$_4$)[Mn$_2$(Im)(edt)$_4$] (**5**)

Mn(1)−S(3)	2.325(3)	Mn(2)−S(16)	2.338(3)
Mn(1)−S(6)	2.342(3)	Mn(2)−S(19)	2.325(3)
Mn(1)−S(7)	2.357(3)	Mn(2)−S(20)	2.341(3)
Mn(1)−S(10)	2.318(3)	Mn(2)−S(23)	2.334(3)
Mn(1)−N(11)	2.197(8)	Mn(2)−N(14)	2.197(7)

S(3)−Mn(1)−S(6)	88.87(11)	S(16)−Mn(2)−S(19)	87.70(10)
S(3)−Mn(1)−S(7)	86.60(10)	S(16)−Mn(2)−S(20)	164.40(11)
S(3)−Mn(1)−S(10)	151.77(12)	S(16)−Mn(2)−S(23)	87.28(10)
S(3)−Mn(1)−N(11)	109.11(21)	S(16)−Mn(2)−N(14)	94.78(20)
S(6)−Mn(1)−S(7)	162.49(12)	S(19)−Mn(2)−S(20)	87.57(10)
S(6)−Mn(1)−S(10)	88.26(10)	S(19)−Mn(2)−S(23)	147.88(11)
S(6)−Mn(1)−N(11)	98.94(21)	S(19)−Mn(2)−N(14)	103.86(21)
S(7)−Mn(1)−S(10)	87.77(10)	S(20)−Mn(2)−S(23)	88.86(10)
S(7)−Mn(1)−N(11)	98.53(21)	S(20)−Mn(2)−N(14)	100.79(20)
S(10)−Mn(1)−N(11)	99.08(21)	S(23)−Mn(2)−N(14)	108.16(21)

increase in the number of bridging atoms, but the ~3.1 Å value is still too long for direct metal−metal bonding.

The anion of **4** (Figure 3) is mononuclear and consists of a five-coordinate Mn^{III} ion with sp geometry ($\tau = 0.11$) and an ImH group occupying the axial position.

The terminal Mn^{III}−S distances (2.315(3)−2.327(3) Å) are similar to those in **3**. The Mn atom lies 0.385 Å above the S$_4$ least-squares plane. The ImH ring is planar, as expected, but tilted slightly such that it forms an angle of 13.52° with the

Mn−N(10) vector. The mononuclear anions are connected into 1-D chains (Figure 4) via NH···S hydrogen bonds between the ImH N−H group of one anion and the S atom S(6) of an adjacent anion (N(12)···S(6) = 3.30(1) Å).

The anion of **5** (Figure 5) is dinuclear and comprises two five-coordinate Mn^{III} ions chelated by edt^{2-} groups and bridged by an imidazolate (Im$^-$) group across a Mn···Mn separation of 6.487(2) Å. The Mn geometries are approximately sp ($\tau = 0.18$ and 0.28 for Mn(1) and Mn(2), respectively) with the Im$^-$ N atoms in the axial positions. The anion of **5** is thus structurally related to that of **4** and has C_{2v} virtual symmetry. Both Mn−N distances are identical (2.197(8) Å) and significantly shorter by 0.027 Å than that in **4** (2.224(7) Å), consistent with stronger binding of Im$^-$ *vs* ImH. A similar difference has been seen in Mn^{III} porphyrin chemistry where the Mn−Im$^-$ distance (2.280(4) Å) in [Mn(Im)(TPP)]$_n$ is 0.028 Å shorter than in [Mn(1-MeIm)$_2$-(TPP)]$^+$ (2.308(3) Å).[22,23] The Mn^{III} ions in **5** are not quite coplanar with the Im$^-$ ring, the deviations being 0.126 and 0.027 Å for Mn(1) and Mn(2), respectively. Mn(1) lies 0.462 Å above the S(3,6,7,10) least-squares plane, and Mn(2) lies 0.481 Å above the S(16,19,20,23) plane; both these values are significantly greater than that in **4** (0.385 Å), again undoubtedly due to the Im$^-$ *vs* ImH binding differences.

The anion of **5** joins a number of other imidazolate-bridged dinuclear complexes in the literature, including, in Mn chemistry, [Mn^{II}$_3$(ImH)$_2$(Im)$_6$]$_n$,[24] [Mn^{III}(Im)(TPP)]$_n$ (TPP = tetraphenylporphyrin dianion),[23] and [Mn^{II}Cu^{II}LL′] (L and L′ are tetradentate ligands).[25] Most other structurally characterized, dinuclear examples are in Cu^{II}$_2$ chemistry,[26−28] with exceptions including Cu^{II}Co^{III},[29] Rh^I$_2$,[30] Cu^{II}Ni^{II},[31] Cu^{II}Zn^{II},[32] and Ni^{II}$_2$[33] species.

Magnetochemical Studies. Variable-temperature magnetic susceptibility data were collected on powdered samples of complexes **1**−**5** in the temperature range 2.00−300 K.

For complexes **1** and **2**, similar values of effective magnetic moment (μ_{eff}) per Mn$_2$ were obtained, being ~5.6 μ_B at 300 K and decreasing steadily to ~0.4 μ_B at 2.00 K (Figure 6). The expected μ_{eff} value for a dinuclear complex with noninteracting Mn^{III} ($S = 2$) ions is 6.93 μ_B, and this together with the near-zero value at 2.00 K suggests the presence of antiferromagnetic exchange interactions in **1** and **2**.

(22) Landrum, J. T.; Hatano, K.; Scheidt, W. R.; Reed, C. A. *J. Am. Chem. Soc.* **1980**, *102*, 6729.
(23) This linear polymer comprises alternating high- and low-spin Mn^{III} centers. We refer to the high-spin Mn−N bond; the low-spin Mn−N bond is 2.186(5) Å.
(24) Lehnert, R.; Seel, F. *Z. Anorg. Allg. Chem.* **1980**, *464*, 187.
(25) Matsumoto, N.; Okawa, H.; Kida, S.; Ogawa, T.; Ohyoshi, A. *Bull. Chem. Soc. Jpn.* **1989**, *62*, 3812.
(26) Strothkamp, K. G.; Lippard, S. J. *Acc. Chem. Res.* **1982**, *15*, 318, and references therein.
(27) (a) Matsumoto, K.; Ooi, S.; Nakao, Y.; Mori, W.; Nakahara, A. *J. Chem. Soc., Dalton Trans.* **1981**, 2045. (b) Kolks, G.; Lippard, S. J. *Acta Crystallogr., Sect. C* **1984**, *C40*, 261. (c) Salata, C. A.; Youinou, M.-T.; Burrows, C. J. *Inorg. Chem.* **1991**, *30*, 3454. (d) Coughlin, P. K.; Martin, A. E.; Dewan, J. C.; Watanabe, E.-I.; Bulkowski, J. E.; Lehn, J.-M.; Lippard, S. J. *Inorg. Chem.* **1984**, *23*, 1004.
(28) Haddad, M. S.; Hendrickson, D. N. *Inorg. Chem.* **1978**, *17*, 2622.
(29) Davis, W. M.; Dewan, J. C.; Lippard, S. J. *Inorg. Chem.* **1981**, *20*, 2928.
(30) Kaiser, S. W.; Saillant, R. B.; Butler, W. M.; Rasmussen, P. G. *Inorg. Chem.* **1976**, *15*, 2681.
(31) Costes, J.-P.; Serra, J.-F.; Dahan, F.; Laurent, J.-P. *Inorg. Chem.* **1986**, *25*, 2790.
(32) Pierre, J.-L.; Chautemps, P.; Refaif, S.; Beguin, C.; El-Marzouki, A.; Serratrice, G.; Saint-Aman, E.; Rey, P. *J. Am. Chem. Soc.* **1995**, *117*, 1965 and references therein.
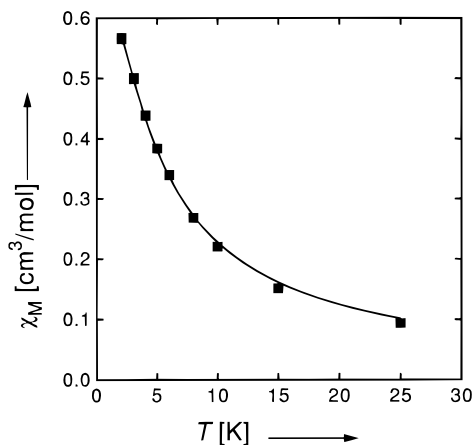(33) Costes, J.-P.; Dahan, F.; Laurent, J.-P. *Inorg. Chem.* **1991**, *30*, 1887.

Figure 6. Plot of the effective magnetic moment, μ_{eff}/mol, *vs* temperature for $(NEt_4)_2[Mn_2(edt)_4]$ (**1**, ▼), $(NEt_3Bz)_2[Mn_2(pttd)_2]$ (**2**, ▲) and $(NMe_4)_3[Mn_2(Im)(edt)_4]$ (**5**, ■) in an applied field of 10.00 kG. The solid lines represent the best fits to the theoretical expression. See text for fitting parameters.

A spin-Hamiltonian was constructed in the limit of an isotropic Zeeman interaction (eq 5). Each Mn^{III} ion has its

$$\hat{H} = \beta \hat{H}_z(g_1\hat{S}_{1z} + g_2\hat{S}_{2z}) - 2J\hat{S}_1\hat{S}_2 +$$
$$D_1(\hat{S}_{1z}^2 - (^1/_3)S_1(S_1 + 1)) + D_2(S_{2z}^2 - (^1/_3)S_2(S_2 + 1)) \quad (5)$$

respective g factor and single-ion axial zero-field splitting parameter (D), with the other terms having their usual meanings. The five parameters (g_1, g_2, D_1, D_2, J) can be reduced to three by using the pseudo-2-fold symmetry of **1** and **2** and setting $g_1 = g_2$ and $D_1 = D_2$. A least-squares fitting program was used[34] which diagonalized the 25×25 Hamiltonian matrix on each cycle and calculated the energy (E_i) and magnetization ($\delta E_i/\delta H$) for each of the 25 microstates. These values were used to calculate χ_M at each temperature point by use of the Van Vleck equation (eq 6),[35] where N is Avogadro's number, k is

$$\chi_M = M/H =$$
$$N\sum(-\delta E_i/\delta H) \exp(-E_i/kT)/H\sum \exp(-E_i/kT) \quad (6)$$

Boltzmann's constant, and H is the applied field. Satisfactory fits of the data for **1** and **2** were obtained by minimizing the relative error between the observed susceptibility (χ_{obs}) and the susceptibility calculated by eq 7, where PAR is the molar

$$\chi_{calc} = (1 - PAR)(\chi_m + TIP) + PAR(2Ng^2\mu_B^2/kT) \quad (7)$$

fraction of paramagnetic impurity, assumed to be mononuclear Mn^{III} ($S = 2$). For **1**, the values were $J = -19.0$ cm^{-1}, $g = 1.96$, $D_1 = D_2 = -0.22$ cm^{-1}, and PAR = 0.37%, with the temperature independent paramagnetism (TIP) held constant at 400×10^{-6} cm^3 mol^{-1}. For **2**, the values were $J = -16.4$ cm^{-1}, $g = 1.96$, $D_1 = D_2 = -0.22$ cm^{-1}, PAR = 0.51%, and TIP the same as for **1**. Both **1** and **2** consequently possess $S = 0$ ground states. Thus, the similarity in the X-ray structures of the cores of **1** and **2** is reflected in the near congruence of their magnetic parameters. As the Mn···Mn separations (>3.5 Å) are too long for significant direct metal−metal interactions, the slightly larger J value of **1** can be correlated with its slightly

(34) Schmitt, E. A. Ph.D. Thesis, 1995, University of Illinois at Urbana-Champaign.
(35) Van Vleck, J. H. *The Theory of Electric and Magnetic Susceptibilities*; Oxford University Press: London, 1932.

Figure 7. Plot of the effective magnetic moment, μ_{eff}/mol, *vs* temperature for $(PPh_4)_2[Mn_3(pdt)_5]$ (**3**, □) in an applied field of 10.00 kG. The solid line represents the best fit to the theoretical expression. See text for fitting parameters.

shorter Mn−S_{br} bond lengths (2.341(2), 2.606(2) Å) compared with **2** (2.353(1), 2.655(1) Å).

For complex **3**, the μ_{eff} decreases steadily from 6.75 μ_B at 300 K to a value of ∼3.9 μ_B below ∼25 K (Figure 7). The calculated μ_{eff} for a trinuclear Mn^{II}, $2Mn^{III}$ complex containing noninteracting metal ions is 9.11 μ_B, suggesting the presence of antiferromagnetic exchange interactions in **3**. Further, the low-temperature μ_{eff} value of ∼3.9 μ_B may be compared with the spin-only ($g = 2$) value for a system with three unpaired electrons ($\mu_{eff} = 3.87$ μ_B), suggesting that **3** has a quartet ($S = {}^3/_2$) ground state; the subsequent fitting of the data supports this.

A model to describe the exchange interactions in **3** was employed that involves two exchange parameters defined by

$$Mn(1) \overset{J_{12}}{\text{---}} Mn(2) \overset{J_{23}}{\text{---}} Mn(3)$$
$$\underset{J_{13}}{\underline{\qquad\qquad\qquad\qquad}}$$

The Heisenberg spin Hamiltonian for this system is given by eq 8; this simplifies to the Hamiltonian in eq 9 on taking $J_{12} =$

$$\hat{H} = -2J_{12}\hat{S}_1\hat{S}_2 - 2J_{23}\hat{S}_2\hat{S}_3 - 2J_{13}\hat{S}_1\hat{S}_3 \quad (8)$$

$$\hat{H} = -2J(\hat{S}_1\hat{S}_2 + \hat{S}_2\hat{S}_3) - 2J'\hat{S}_1\hat{S}_3 \quad (9)$$

$J_{23} = J$, as suggested by the virtual C_2 symmetry of the complex, and $J_{13} = J'$. Using the Kambe vector coupling method[36] and the substitutions $\tilde{S}_A = \hat{S}_1 + \hat{S}_3$ and $\hat{S}_T = \hat{S}_A + \hat{S}_2$, the Hamiltonian of eq 9 can be expressed in the equivalent form given by eq 10, where $S_1 = S_3 = 2$, $S_2 = {}^5/_2$, and S_T is the total

$$\hat{H} = -J(\hat{S}_T^2 - \hat{S}_A^2 - \hat{S}_2^2) - J'(\hat{S}_A^2 - \hat{S}_1^2 - \hat{S}_3^2) \quad (10)$$

$$E(S_T,S_A) = -J[S_T(S_T + 1) - S_A(S_A + 1)] - J'[S_A(S_A + 1)] \quad (11)$$

spin of the complex. The energies of each possible S_T state are given by eq 11, where the $S_i(S_i + 1)$ ($i = 1, 2, 3$) terms contributing to all states have been ignored. Using eq 11 and the Van Vleck equation, a theoretical χ_M *vs* T expression was obtained[37] and used to fit the data for **3** including a term for TIP. Our fitting program minimizes the relative error between μ_{eff} (obs) and μ_{eff} (calc) by varying up to four parameters: g, TIP, J and J'. In fact, g was fixed at 2.00 and TIP was fixed

(36) Kambe, K. *J. Phys. Soc. Jpn.* **1950**, *5*, 48.
(37) See Supporting Information.

Figure 8. Plot of the molar paramagnetic susceptibility, χ_m, *vs* temperature for $(NEt_4)[Mn(edt)_2(ImH)]$ (**4**, ■) in an applied field of 10.00 kG. The solid line represents the best fit to the theoretical expression. See text for fitting parameters.

at 600×10^{-6} cm^3 mol^{-1}; the resultant fit gave a value of J' of ~0, and J' was therefore fixed at zero. With J as the only adjustable parameter, an excellent fit was obtained (Figure 7) with $J = -18.8$ cm^{-1}. Allowing J' to vary leads to insignificant changes to the quality of the fit or the J value.

The complex has 21 possible spin states with S_T values in the $^{13}/_2$ to $^{1}/_2$ range. The above fit shows the ground state to be, in the format (S_T, S_A), the $(^{3}/_2, 4)$ state: The first excited state is the degenerate pair of $(^{5}/_2, 4)$ and $(^{1}/_2, 3)$ states at an energy of $-5J$ or 94.0 cm^{-1} above the ground state, and the second excited state is the $(^{3}/_2, 3)$ state at $-8J$ or 150.4 cm^{-1} above the ground state. The $S_T = ^{3}/_2$ ground state of complex **3** is thus energetically well isolated from the nearest excited states and corresponds to the individual spin alignments shown:

$$\uparrow 2 \qquad \downarrow 5/2 \qquad \uparrow 2$$

$$\text{Mn(1)} \text{------} \text{Mn(2)} \text{-----} \text{Mn(3)}$$
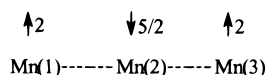
For complex **4**, the μ_{eff} gradually decreases from 4.97 μ_B at 300 K to 4.32 μ_B at 25.0 K and then decreases rapidly to 3.05 μ_B at 2.05 K. The 300 K value agrees with the expected spin-only value of 4.90 μ_B for a high-spin Mn^{III} (d^4) ion, consistent with the mononuclear, Mn^{III} nature of **4**. The free ion ground state of Mn^{III} is ^5D, which, in an axially-elongated tetragonal field, splits into a $^5B_1$ ground state and low-lying $^5A_1$, ^5E, and $^5B_2$ excited states.[38a] Additionally, for a Mn^{III} ion in the $^5B_1$ ground state, the sign of the zero-field splitting parameter D is always negative due to a crystal-field argument.[38b] For a Mn^{III} ion in a $^5B_1$ state, the spin-only effective magnetic moment is calculated to be $\mu_{eff} = [g^2 S(S + 1)]^{1/2} = 4.90$ μ_B for $g = 2$. This value of 4.90 μ_B should be observed as a constant over a wide temperature range. However, for **4**, this is not the case. The gradual decrease in μ_{eff} as temperature is decreased from 300 to 25.0 K is indicative not of magnetic exchange interactions but most likely a nonzero orbital contribution to the effective magnetic moment. This spin–orbit admixture of the ^5E state into the $^5B_1$ ground state is difficult to numerically account for, but it has been seen in other Mn^{III} complexes.[22,39] In contrast, the rapid decrease in μ_{eff} below 25.0 K could be due to two things: single ion zero-field splitting effects or intermolecular

interactions. It is possible to fit the low-temperature data to a zero-field splitting model; however, such a fit gives a value of $D > 0$, which is unreasonable in light of the electronic structure of Mn^{III}. A more reasonable explanation involves a weak magnetic exchange propagated along the hydrogen-bonding network of the solid. This hydrogen bonding occurs between the distal hydrogen of the apical imidazole and a sulfur atom ligated to an adjacent complex of **4**, forming 1-D chains along the crystallographic *b* axis (Figure 4).

A Heisenberg Hamiltonian for magnetic exchange was used following Fisher's model, $\hat{H} = -2J\sum \hat{S}_i \hat{S}_{i+1}$, with the spins treated as classical spins.[40] Briefly, this model permits each of the $S = 2$ spins to have a continuum of values rather than the discrete $m_s = \pm 2, \pm 1, 0$ values permitted by quantum mechanics. This permits the derivation of an analytical expression for χ_m [40] and is reasonable given both the relatively large single-ion spin value of $S = 2$ and the infinite nature of a chain. A least-squares fitting to the data from 2.00 to 25.0 K yielded the solid line seen in Figure 8, with values of $J = -0.15$ cm^{-1} and $g = 1.91$, which tracks the data quite well over this range. It must be noted that since this model does not account for the spin–orbit admixture of the ^5E state into the $^5B_1$ ground state for **4**, it cannot account for the high-temperature data. This orbital contribution is approximated in the low-temperature fit by allowing g to deviate from 2.00. Orbital contributions to the moment are expected to reduce g from 2.00 for Mn^{III} (less than half-filled shell), which is in accord with our fit.

For complex **5**, the μ_{eff} steadily decreases from 6.38 μ_B at 300 K to 1.57 μ_B at 2.00 K (Figure 6), again consistent with the presence of antiferromagnetic exchange interactions. Preliminary fitting of the data using an isotropic Heisenberg Hamiltonian ($\hat{H} = -2J\hat{S}_1\hat{S}_2$) gave $J = -1.90$ cm^{-1} and $g = 1.84$, but by the neglecting of zero-field splitting effects this fit overestimates the value of J. Zero-field splitting for Mn^{III} compounds is typically small but can be on the order of a few wavenumbers[37,41] and, therefore, could have a significant impact upon the fitting when the exchange interaction is so weak. It was necessary to diagonalize the full Hamiltonian matrix, accounting for the Zeeman interaction, magnetic exchange, and single-ion zero-field splitting effects, in order to account fully for the magnetic behavior of **5**. This was performed using the same procedure as for **1** and **2** employing eqs 5 and 6, and this gave a good fit with $J = -1.75$ cm^{-1}, $g = 1.84$, $D_1 = D_2 = -0.0282$ cm^{-1}, and PAR = 1.3%, with TIP held constant at 400×10^{-6} cm^3 mol^{-1}. It should be noted that the sign of D in **5** (and also **1**–**4**) is not uniquely determined by the fits but rather by the $^5B_1$ ground state of each Mn^{III} in near square-pyramidal geometry. The rather low g value is probably a result of orbital contributions to the moment, as discussed earlier, and other minor effects, such as weak, intermolecular interactions, that are not taken into account by our model.

Solution Studies. The solution behavior of **1** has been described previously and is consistent with dissociation of the $[Mn_2(edt)_4]^{2-}$ into solvated mononuclear units (eq 12) in good

$$[Mn_2(edt)_4]^{2-} + n \text{ solv} \rightleftharpoons 2[Mn(edt)_2(solv)_n]^- \quad (12)$$
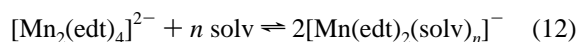
donor solvents.[13,14] Complex **2** shows similar behavior. In contrast, complex **3** shows no evidence of dissociation in solution into smaller units. For example, the electronic spectrum

(38) (a) Kennedy, B. J.; Murray, K. S. *Inorg. Chem.* **1985**, *24*, 1552. (b) Mitra, S. *Chem. Phys. Lett.* **1984**, *104*, 353.

(39) Gregson, A. K.; Doddrell, D. M.; Healy, P. C. *Inorg. Chem.* **1978**, *17*, 1216.

(40) (a) Fisher, M. E. *Am. J. Phys.* **1964**, *32*, 343. (b) De Munno, G.; Julve, M.; Real, J. A.; Lloret, F.; Scopelliti, R. *Inorg. Chim. Acta* **1996**, *250*, 81.

(41) Mitra, S.; Rehere, D. V. *Inorg. Chem.* **1980**, *19*, 992.

is not concentration-dependent and the solution μ_{eff} is invariant at 7.13 ± 0.02 μ_B in DMSO in the concentration range 0.84–1.60 mM; the μ_{eff} value expected for complete dissociation into Mn^{II} and $2Mn^{III}$ ions is 9.11 μ_B per Mn_3. The 7.13 μ_B solution value at room temperature is slightly higher than the solid-state value (by ~6%), perhaps due to experimental error in the determination by the Evans method or maybe small changes to the bridging angles (and hence J and μ_{eff}) on dissolution.

For **4** in DMSO and MeCN, solution μ_{eff} values in the range 4.85–5.05 μ_B have been obtained. These are similar to the solid-state value (4.97 μ_B) and are consistent with a high-spin ($S = 2$) Mn^{III} center. The solvolysis equilibrium of eq 13 would

$$[Mn(edt)_2(ImH)]^- + n \text{ solv} \rightleftharpoons [Mn(edt)_2(solv)_n]^- + ImH \tag{13}$$
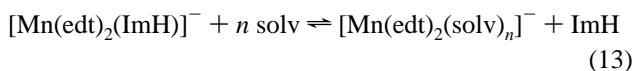
no doubt be operating in these good donor solvents, but this would obviously not be reflected in the magnetic moments unless a spin change associated with conversion to a low-spin ($S = 1$) center were occurring, but this would not be expected with such weak field ligands. Note that cleavage of the Mn^{III}–ImH bond in good donor solvents was established by recrystallization of **4** from DMF/THF, which yielded **1**.[13b]

The solution μ_{eff} value of **5** is 6.45 μ_B, in good agreement with the solid-state value (6.38 μ_B). Since **5** is dinuclear, this rules out the occurrence to any noticeable extent of the solvolysis equilibrium of eq 14. Severage of the bridge to yield solvated

$$[Mn_2(Im)(edt)_4]^{3-} + 2n \text{ solv} \rightleftharpoons 2[Mn(edt)_2(solv)_n]^- + Im^- \tag{14}$$
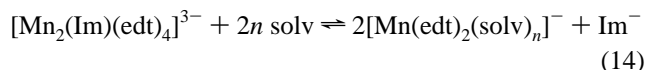
monomers would be expected to result in increased moments approaching the limiting value of **4** and with the observed moments also being concentration-dependent as the position of equilibrium is affected; no evidence for this is seen. The solution values thus support retention in solution of the solid-state structure of **5**. This is consistent with the observed structural differences between **4** and **5** and the fact that **5** can be recrystallized without change from DMF/THF.

Discussion

The aerial oxidation of reaction mixtures comprising Mn^{II} and dithiolates capable of forming five- or six-membered chelate rings allows access to a family of Mn^{III}/dithiolate species. The $[Mn_3(pdt)_5]^{2-}$ ion appears to be at the border of thermal stability, with the butane-1,4-dithiolate product being too unstable for isolation at reasonable temperatures (>0 °C). Unfortunately, use of mixed S/O or S/N ligands capable of forming five-membered chelate rings also gave decreased product stability *vis-à-vis* complexes with edt^{2-}, pdt^{2-}, or related dithiolate groups.

Magnetic characterization revealed all exchange interactions in **1**–**5** to be antiferromagnetic in nature and thus to lead to small or zero ground-state spin values. The J values of −19.0 and −16.4 cm^{-1} for **1** and **2**, respectively, show that the slight structural differences in the $[Mn_2S_2]$ cores lead to only very small differences in the resulting exchange interactions. In contrast, the value for **1** may be compared with the significantly stronger interaction ($J = -54$ cm^{-1}) in the $[Fe_2(edt)_4]^{2-}$ (**6**) anion,[42] which has essentially the same structure as the anion of **1**. If **6** contains high-spin ($S = 5/2$) Fe^{III} ions, then the stronger coupling could reasonably be attributed to the extra singly-

populated d_σ orbital compared with Mn^{III} ($S = 2$). Anion **6** would have $M-S_{br}-M$ (br = bridging) σ overlaps between d_σ magnetic orbitals that are not present in **1** due to the centrosymmetric structure and only half of the d_σ orbitals being populated. If the $M-S_{br}-M$ σ overlaps lead to increased antiferromagnetic contributions to the overall J, then that would rationalize the stronger antiferromaganetic interaction in **6** *vs* **1**. We note, however, that it has been suggested that **6** contains intermediate-spin ($S = 3/2$) Fe^{III} ions,[14b] in which case **6** would contain fewer d_π magnetic orbitals than **1**. In this case, the stronger antiferromagnetic coupling in **6** *vs* **1** might be due not to an increase in antiferromagnetic contributions but to a decrease in ferromagnetic contributions from a "crossed pathway" [43] involving overlap of singly-occupied d_π orbitals on one M with empty d_σ orbitals on the other. In fact, this argument would also be applicable even if both Fe^{III} ions were high-spin, since no empty d_σ orbitals would then be available. The importance of "crossed pathway" interactions between singly-occupied d_π and empty d_σ orbitals was recently proposed[44] as the origin of the overall *ferro*magnetic interactions ($J = +43.5$ cm^{-1}) between adjacent V^{III} ions in $[V_3Cl_6(edt)_3]^{3-}$.

The antiferromagnetic exchange interaction in **3** ($J = -18.8$ cm^{-1}) is essentially identical with that in **1** and **2** and consistent with both σ and π overlaps of magnetic orbitals providing antiferromagnetic contributions which dominate the few possible ferromagnetic pathways. Similarly, the very weak antiferromagnetic inter- and intramolecular exchange interactions in **4** and **5**, respectively, are consistent with their structures. The extreme weakness of the antiferromagnetic exchange interaction observed for the imidazolate-bridged anion in **5** is in agreement with previous studies of exchange interactions in imidazolate-bridged complexes. The first nonpolymeric complex with imidazolate bridging between two Cu^{II} ions, tetrameric $[Cu_2(bpim)(Im)]_2(NO_3)_4 \cdot 4H_2O$ (bpim is 4,5-bis[[(2-(2-pyridyl)ethyl)-imino)methyl]limidazolate) was reported in 1976.[45] In the following years, the preparation and characterization of many other dinuclear Cu^{II} complexes bridged by imidazolate, 2-methylimidazolate, benzimidazolate, biimidazolate (BiIm), and bibenzimidazolate (BiBzim) were reported.[28,46] All of the complexes exhibit antiferromagnetic interactions, with the J values ranging from $|J| < 0.5$ cm^{-1} to as large as $J = -87.6$ cm^{-1}. Imidazolate-propagated magnetic exchange interactions have also been reported for other metal ions. The antiferromagnetic exchange interactions between the two d^1 (η^5-C_5H_5)$_2Ti^{III}$ moieties in $[(Cp)_2Ti]_2(BiIm)$ and $[(Cp)_2Ti]_2(BiBzim)$ have been found to have J values of −25.2 and −19.2 cm^{-1}, respectively.[47] Imidazolate-bridged dinuclear face-to-face porphyrin complexes with either high-spin (hs)$Fe^{II}-Im-Fe^{II}$ or (hs)$Mn^{II}-Im-(ls)-Co^{II}$ configurations have J values of −2.3 and −5 cm^{-1}, respectively.[48] Finally, the magnitude of $-J$ observed for the

(42) Herskovitz, T.; De Pamphilis, B. V.; Gillum, W. O.; Holm, R. H. *Inorg. Chem.* **1975**, *14*, 1426.

(43) Hotzelmann, R.; Wieghardt, K.; Flörke, U.; Haupt, H.-J.; Weatherburn, D. C.; Bonvoisin, J.; Blondin, G.; Girerd, J.-J. *J. Am. Chem. Soc.* **1992**, *114*, 1681.

(44) Rambo, J. R.; Castro, S. L.; Folting, K.; Bartley, S. L.; Heintz, R. A.; Christou, G. *Inorg. Chem.* **1996**, *35*, 6844.

(45) Kolks, G.; Frihart, C. R.; Rabinowitz, H. N.; Lippard, S. J. *J. Am. Chem. Soc.* **1976**, *98*, 5720.

(46) (a) Kolks, G.; Lippard, S. J. *J. Am. Chem. Soc.* **1977**, *99*, 5804. (b) Haddad, M. S.; Duester, E. N.; Hendrickson, D. N. *Inorg. Chem.* **1978**, *18*, 141. (c) Hendricks, H. M. J.; Reedijk, J. *Inorg. Chim. Acta* **1979**, *37*, L509.

(47) Fieselmann, B. F.; Hendrickson, D. N.; Stucky, G. D. *Inorg. Chem.* **1978**, *17*, 2078.

(48) Landrum, J. T.; Grimmett, D.; Haller, K. J.; Scheidt, W. R.; Reed, C. A. *J. Am. Chem. Soc.* **1981**, *103*, 2640.

low-spin imidazolate polymers $[M^{III}(Im)(TPP)]_n$ (M = Fe or Mn) has been reported[22] as being equal to essentially zero.

It is generally agreed that the dominant magnetic exchange interaction pathway for imidazolate-bridged complexes is a σ orbital based pathway.[28,46b] Unpaired electron density in metal σ orbitals that are oriented properly to interact with the nitrogen lone pair orbitals of the imidazolate ion will lead to appreciable antiferromagnetic exchange interactions. In the case of the dinuclear Cu^{II} complexes, several factors which influence the magnitude of $-J$ have been identified, such as changes in the ground state from $d_{x^2-y^2}^1$ to $d_{z^2}^1$ and changes in the spectator ligands. Basically, this results from changes in the orientation of the unpaired-electron-containing metal orbital relative to the imidazolate bridge. On the other hand, the magnitude of this antiferromagnetic interaction is reduced when the metals have electron density in d_π orbitals that can interact with the π system of the imidazolate bridge, such as the $[Fe^{II}_2(\mu\text{-}Im)]$ and $[Mn^{II}\text{-}Co^{II}(\mu\text{-}Im)]$ species mentioned above or the $[Mn^{III}(Im)(TPP)]_n$ polymer. In **5**, the sp Mn^{III} ions will have the configuration $d_{xz}^1 d_{yz}^1 d_{xy}^1 d_{z^2}^1$ (z axis along Mn$-$N bond) and both σ and π exchange pathways are thus possible. A small exchange parameter is thus observed.

Conclusions

The use of dithiolate ligands allows access to a family of Mn^{III}-containing species, but the antiferromagnetic exchange interactions lead to low values of ground state spin, and thus this area of Mn^{III} chemistry does not appear at this time to be a source of new high-spin molecules. Just as importantly *vis-à-vis* the objectives stated in the Introduction, the zero-field splitting parameter D for **3**, which has a nonzero ground state ($S = \frac{3}{2}$), is likely $|D| \leq 0.25$ cm^{-1}, given the values found for **1** and **2**. The calculated barrier to relaxation in **3** could thus be as high as $(S^2 - \frac{1}{4})D = 0.5$ cm^{-1}, but this is still at least 1 order of magnitude less than required for the observation of out-of-phase signals in AC susceptibility studies.[3-6,10-12] We thus conclude that Mn^{III}/S chemistry is an interesting subarea of Mn^{III} coordination chemistry but not one that will provide a new source of single-molecule magnets, at least not with the nuclearities or topologies seen to date. Higher nuclearity species with topologies that introduce competing exchange interactions would, however, be one way to obtain high ground state spin values with antiferromagnetic exchange interactions.

Supporting Information Available: Textual and tabular summaries of the structure determinations, tables of atomic coordinates, thermal parameters, and bond distances and angles, fully labeled figures for complexes **2**-**5** and the χ_m *vs* T equation for **3** (68 pages). Ordering information is given on any current masthead page.

IC970587R